Magnetothermal properties of $\mathbf{Tm_xDy_{1-x}Al_2}$ ($x = 0.25, 0.50$ and 0.75)

P. O. Ribeiro[1,2], B. P. Alho[2,3], R. S. de Oliveira[3], E . P. Nóbrega[3], V. S. R. de Sousa[3], P. J. von Ranke[3], Y. Mudryk[2], V.K. Pecharsky[2,4]

[1] Instituto de Aplicação Fernando Rodrigues da Silveira, Universidade do Estado do Rio de Janeiro – UERJ, Rua Santa Alexandrina 288, 20261-232 RJ, Brazil.
[2] The Ames Laboratory, U.S. Department of Energy, Iowa State University, Ames, IA, 50011-2416, USA.
[3] Instituto de Física, Universidade do Estado do Rio de Janeiro - UERJ, Rua São Francisco Xavier, 524, 20550-013, RJ, Brazil.
[4] Department of Materials Science and Engineering, Iowa State University, Ames, IA, 50011-1096, USA.

E-mail: paula.ribeiro@gmail.com

Abstract

We describe magnetic, thermal, and magnetocaloric properties of rare earth intermetallic compounds $Tm_xDy_{1-x}Al_2$ with $x = 0.25$, 0.5 and 0.75. Using model Hamiltonian we consider contributions of the crystalline electric field anisotropy in both Tm and Dy magnetic sublattices, disorder in exchange interactions among Tm-Tm, Dy-Dy and Tm-Dy magnetic ions, and the Zeeman effect. Employing earlier reported and new experimental measurements, we first determine a single free variable – the intersublattice magnetic exchange parameter – to properly model the temperature and magnetic field dependencies of heat capacity and magnetization, and then use the modeling results to explain the emergence of an anomalous spin reorientation transition and its influence on the magnetocaloric effect in the title compounds. Theoretical results agree with experimental data reasonably well.

Keywords: heat capacity; magnetocaloric effect; intermetallic compounds; magnetic anisotropy.

1. Introduction

Refrigeration technologies in use today are primarily based on a vapor-compression cycle that utilizes volatile liquids, such as hydrofluorocarbons (HCFCs). As a result, routine releases of conventional refrigerants, some of which have the global warming potential orders of magnitude higher than carbon dioxide, into the atmosphere from the aging cooling equipment and from accidents are all but inevitable. One of the grand challenges for the modern science and technology is, therefore, finding a suitable replacement for the vapor-compression, for example by developing approaches that can employ solid refrigerants as environmentally benign alternatives to HCFCs. To

assist with this goal, it is necessary to discover novel refrigerant (caloric) solids, which will enable cost-effective and energy-efficient solid-state refrigeration [1–8].

Performance of caloric materials is typically characterized by two thermodynamic parameters, namely isothermal entropy change (ΔS_T) and adiabatic temperature change (ΔT_{ad}), which are reported for a given external field change across the potential working temperature window of a cooling system. The actuating external field can be magnetic, then thermal response of a solid is known as magnetocaloric effect (MCE) [9, 10], electric (electrocaloric effect) [11], pressure (barocaloric effect) [12], and stress (elastocaloric effect) [13]. The last two phenomena together are also called mechanocaloric effects. Among the different kinds of caloric effects, the most broadly studied is MCE, which dates back to 1917 when Weiss and Piccard [14] reported a reversible temperature change in elemental nickel close to its Curie temperature, rationalized later by Debye [15] and Giauque [16]. The first application of the phenomenon was demonstrated in the cryogenic regime by Giauque and McDougal [17], and it is now common in laboratory setting to reach millikelvin temperatures. Following the discovery of the giant magnetocaloric effect in $Gd_5Si_2Ge_2$ in 1997 [18], the focus has shifted to identifying new solids for potential use as refrigerants in devices operating near room temperature [6, 19–22]. Regardless of the temperature range or the application, there remains a strong interest in understanding fundamental physical behaviors of magnetic materials through determination and analysis of their magnetocaloric properties with the goal to both understand experimental results and accelerate development of new materials [7, 8, 23].

One family of compounds that has emerged as an excellent model system for theoretical and experimental investigations of magnetocaloric behavior is RAl_2, where R is one or more of 16 naturally occurring rare earth elements. Here, localized 4f magnetic moments are associated exclusively with the R-sites in highly symmetric and nearly isotropic cubic crystal lattices that support long-range ferromagnetism with the exception of R = Sc, Y, La, and Lu. Further, dialuminides of rare earths are relatively easy to synthesize in both polycrystalline and single-crystalline forms. Finally, a number of reports describe interesting physical behaviors of both binary RAl_2 compounds and pseudobinary $R_{1-x}R'_xAl_2$ solid solutions, showing the important contributions of the crystalline electric field (CEF) anisotropy on the magnetic and magnetocaloric properties of these compounds [24–26].

In this work, we report theoretical and experimental investigation of how magnetocrystalline anisotropy affects magnetism and magnetothermal behavior, and MCE in the ferromagnetic pseudobinary system $Tm_xDy_{1-x}Al_2$ with x = 0.25, 0.5 and 0.75. The properties of the binary parents (x = 0 and x = 1.0) have already been broadly studied both experimentally and theoretically [27–31]. The three studied compounds exhibit high magnetocaloric effects between 47.9 K for x = 0.25 and 15.8 K and for x = 0.75, respectively [32]. It was predicted that $DyAl_2$ should exhibit strong anisotropic MCE around its spin reorientation temperature, T_R, exceeding conventional magnetocaloric effect around its Curie temperature, T_C [33]. For $TmAl_2$ there is experimental evidence [34] of a spin reorientation transition below T_C, but it vanishes in the investigated intermediate $Tm_xDy_{1-x}Al_2$ compounds with x = 0.25, 0.50 and 0.75 [32]. Making use of a microscopic theoretical model, which includes magnetic exchange, CEF, and Zeeman interactions,

we predict anisotropic magnetization and spin reorientations in both the Tm and Dy sublattices, and validate theoretical predictions of magnetocaloric effect with experiments.

2. Experimental

Polycrystalline samples used for heat capacity measurements were taken from the same alloys that were originally described in reference [32]. The heat capacity was measured using the relaxation technique in a Quantum Design, Inc. Physical Property Measurement System (PPMS). The measurements were performed between 2 and 100 K for $x = 0.25$ and between 2 and 80 K for $x = 0.50$ and 0.75 in magnetic fields $\mu_0 H = 0$, 1, and 2 T, where μ_0 is the magnetic permeability of vacuum and H is the magnetic field strength. The zero field data, as expected, match the data reported in Ref. 32. All magnetic ordering phase transitions in the studied compounds are second order, and they broaden significantly upon application of magnetic field.

3. Theory

In order to describe the magnetic properties of cubic C15 Laves-phase series of $Tm_xDy_{1-x}Al_2$ compounds, whose magnetism arises from the presence of two rare earth sublattices, Tm^{+3} and Dy^{+3}, the model Hamiltonians in the mean field approximation are given by:

$$\mathcal{H}^{\mathrm{Tm}} = -g^{\mathrm{Tm}}\mu_B[x\lambda^{\mathrm{Tm}}\vec{M}^{\mathrm{Tm}} + x(1-x)\lambda^{\mathrm{TmDy}}\vec{M}^{\mathrm{Dy}} + \mu_0\vec{H}]\cdot\vec{J}^{\mathrm{Tm}} + \mathcal{H}_{\mathrm{CEF}}^{\mathrm{Tm}}, \quad (1)$$

$$\mathcal{H}^{\mathrm{Dy}} = -g^{\mathrm{Dy}}\mu_B[(1-x)\lambda^{\mathrm{Dy}}\vec{M}^{\mathrm{Dy}} + x(1-x)\lambda^{\mathrm{TmDy}}\vec{M}^{\mathrm{Tm}} + \mu_0\vec{H}]\cdot\vec{J}^{\mathrm{Dy}} + \mathcal{H}_{\mathrm{CEF}}^{\mathrm{Dy}}. \quad (2)$$

Here, μ_B is the Bohr magneton, $g^{\mathrm{Tm}} = 7/6$, $g^{\mathrm{Dy}} = 4/3$ and $\vec{J}^{\mathrm{Tm}}$, $\vec{J}^{\mathrm{Dy}}$ are the corresponding Landé factors and total angular momentum operators, respectively, and λ is the mean field parameter quantifying exchange interactions. The first two terms inside the brackets in (1) and (2) account for disorder [35, 36] by considering exchange interactions between the same [$x\lambda^{\mathrm{Tm}}$ and $(1-x)\lambda^{\mathrm{Dy}}$] or different sublattices [$x(1-x)\lambda^{\mathrm{TmDy}}$], where x is the concentration of Tm. The third term in the brackets accounts for the Zeeman interactions where $\mu_0\vec{H}$ is the applied magnetic field. The last terms in (1) and (2) represent the crystalline electric field (CEF) interactions, which can be written for cubic symmetry in Lea, Leask, and Wolf (LLW) notation [37] for each rare-earth sublattice (R = Tm or Dy) as:

$$\mathcal{H}_{\mathrm{CEF}}^{\mathrm{R}} = W^{\mathrm{R}}\left[X^{\mathrm{R}}\left(\frac{O_4^0+5O_4^4}{F_4}\right)^{\mathrm{R}} + (1-|X^{\mathrm{R}}|)\left(\frac{O_6^0-21O_6^4}{F_6}\right)^{\mathrm{R}}\right]. \quad (3)$$

In (3), W is the energy scale, and X is limited to the range $-1 \le X \le 1$, giving the ratio between the fourth- and sixth-order Steven's operators O_n^m [38, 39]. F_4 and F_6 are multiplicative factors

common to all matrix elements and specific for each total angular momentum *J* as tabulated by LLW [37].

From the Hamiltonians (1) and (2), the eigenvectors ($|\varepsilon_n^{\mathrm{R}}\rangle$, and eigenvalues ($\varepsilon_n^{\mathrm{R}}$), of each rare-earth sublattice (R = Tm or Dy), are obtained and the components of the magnetization along three crystal axes ($i = x, y$, or z directions) are calculated by the Boltzmann thermodynamic mean value of the magnetic moments ($g^R \mu_B J_i^{\mathrm{R}}$) as follows:

$$M_i^{\mathrm{R}} = g^{\mathrm{R}} \mu_B \frac{\sum_n \langle \varepsilon_n^{\mathrm{R}} | J_i^{\mathrm{R}} | \varepsilon_n^{\mathrm{R}} \rangle e^{\left(-\beta \varepsilon_n^{\mathrm{R}}\right)}}{\sum_n e^{\left(-\beta \varepsilon_n^{\mathrm{R}}\right)}}, \tag{4}$$

where $\beta = 1/k_B T$ and k_B is the Boltzmann constant.

Three main contributions to the total entropy were considered: for each rare-earth sublattice, the magnetism of rare earth ions, $\left(S_{mag}^{\mathrm{R}}\right)$, the lattice contribution from phonons (S_{lat}), and conduction electron entropy (S_{el}). The first of them can be expressed as:

$$S_{mag}^{\mathrm{R}}(T, \mu_0 H) = \mathcal{R}\left[ln \sum_i e^{-\beta \epsilon_i^{\mathrm{R}}} + \beta \frac{\sum_i \epsilon_i^{\mathrm{R}} e^{-\beta \epsilon_i^{\mathrm{R}}}}{\sum_i e^{-\beta \epsilon_i^{\mathrm{R}}}}\right], \tag{5}$$

where $\mathcal{R}$ is the gas constant. The lattice vibration contribution to the total entropy, in the Debye approximation, is given by:

$$S_{lat}(T) = N_A \mathcal{R}\left[-3 \ln\left(1 - e^{\frac{\theta_D}{T}}\right) + 12\left(\frac{T}{\theta_D}\right)^3 \int_0^{\theta_D/T} \frac{y^3}{e^y - 1} dy\right]. \tag{6}$$

Where θ_D is the Debye temperature and $N_A = 3$ is the number of atoms in the formula unit. As described in the literature [27, 28], θ_D in the RAl_2 series of compounds can be approximated by a linear combination, where n is defined as $0 \leq n \leq 14$, and n = 0 for La, and n = 14 for Lu:

$$\theta_D^{\mathrm{RAl_2}}(T, n) = \frac{[14-n]\, \theta_D^{\mathrm{LaAl_2}}(T) + n \theta_D^{\mathrm{LuAl_2}}(T)}{14}. \tag{7}$$

In the present case, $n = 12$ for $TmAl_2$ and $n = 9$ for $DyAl_2$, and the functions $\theta_D^{\mathrm{LaAl_2}}(T)$ and $\theta_D^{\mathrm{LuAl_2}}(T)$ were taken from the literature [28]. For the pseudobinary $Tm_xDy_{1-x}Al_2$:

$$\theta_D^{\mathrm{Tm_xDy_{1-x}Al_2}}(T, x) = x \theta_D^{\mathrm{TmAl_2}}(T, x) + (1 - x) \theta_D^{\mathrm{DyAl_2}}(T, x). \tag{8}$$

The last term of the total entropy, electronic contribution, can be written as:

$$S_{el}(T) = \bar{\gamma} T, \tag{9}$$

where $\bar{\gamma}$ corresponds to an effective Sommerfeld coefficient. As we have done for $\theta_D(T,x)$, the electronic entropy was calculated assuming a linear change across the series from the nonmagnetic La to the nonmagnetic Lu. The values of $\bar{\gamma}^{\mathrm{LaAl_2}} = 10.6$ mJ/mol·K and $\bar{\gamma}^{\mathrm{LuAl_2}} = 5.5$ mJ/mol·K were taken from a previous work [40]. As for the other quantities, the disorder effect was included in the total entropy, given by:

$$S_{total}(T,\mu_0 H,x) = (x)S_{total}^{\mathrm{Tm}} + (1-x)S_{total}^{\mathrm{Dy}}. \quad (10)$$

From the total entropy, the MCE parameters can be calculated from the relations:

$$\Delta S_T(T,H) = S_{total}(T,\mu_0 H \neq 0) - S_{total}(T,\mu_0 H = 0), \quad (11)$$

and

$$\Delta T_{ad}(T,H) = T_2(S,\mu_0 H \neq 0) - T_1(S,\mu_0 H = 0). \quad (12)$$

Experimentally, ΔS_T and ΔT_{ad} for a given magnetic field change, $\mu_0 \Delta H$, can be calculated from heat capacity, $C_p(T,\mu_0 H)$, measured as function of temperature in constant $\mu_0 H = 0$ and $\mu_0 H \neq 0$ as isothermal (Eq. 11) and isentropic (Eq. 12) differences between the total entropy functions defined as $S_{total}^{exp.}(T,\mu_0 H) = \int_0^T \left(C_p(T,\mu_0 H)/T\right)dT$ [41].

4. Application and discussion

The $\mathrm{Tm}_x\mathrm{Dy}_{1-x}\mathrm{Al}_2$ compounds crystallize in the C15 cubic Laves phase structure and the easy magnetization directions at the ground states are $\langle 110\rangle$ and $\langle 001\rangle$ for the binary $TmAl_2$ and $DyAl_2$, respectively [42, 43]. In order to apply the model described in Section 3 to study the pseudobinaries with x = 0.25, 0.50 and 0.75, a few assumptions regarding the crystal structure; and CEF (X and W) and exchange parameters (λ) are required.

We assume that Dy and Tm in the $\mathrm{Tm}_x\mathrm{Dy}_{1-x}\mathrm{Al}_2$ solid solution replace one another and neither replaces Al. This assumption is supported by the available body of knowledge about chemistry and crystallography of intermetallic compounds of rare earths with Al, hence both lanthanide ions only have Al in their nearest coordination spheres [44, 45]. We also assume that the CEF interactions of Tm and Dy with the ligands do not deviate significantly from the ones present in the binary compounds. Hence, the crystal field parameters were kept constant for all intermediate concentrations using the corresponding values reported for binary $TmAl_2$ and $DyAl_2$. The exchange parameters, λ^{Tm} and λ^{Dy}, were adjusted to reflect the experimentally observed transition temperatures, namely $T_C \cong 3.8$ K for $TmAl_2$ and $T_C \cong 62.1$ K for $DyAl_2$ known from the literature [32], and then kept constant as well. Hence, the model has only a single free parameter – λ^{TmDy}, the

intersublattice exchange parameter – that was adjusted to best reproduce the experimentally observed ferromagnetic ordering temperatures for the three compounds with x = 0.25, 0.5, and 0.75. This parameter takes into account the intersublattice exchange interactions, and it is responsible for the coupling between the two magnetic sublattices.

The exchange and CEF parameters used in the model are listed in Tables 1 and 2. The eigenvectors and eigenvalues of Hamiltonians (1) and (2) are obtained self-consistently for a fixed temperature and magnetic field. The magnetization of the Tm sublattice is set initially parallel to the $\langle 110 \rangle$ direction and that of the Dy sublattice parallel to the $\langle 001 \rangle$, but they are free to rotate during the self-consistent procedure.

Figure 1 shows good agreement between measured and modelled heat capacities as functions of temperature for x = 0.25 (Fig. 1a), x = 0.5 (Fig. 1b) and x = 0.75 (Fig. 1c) in magnetic fields of 0 and 2 T (the same in magnetic field of 1 T is illustrated in the supplementary material, Fig. S1). As noted in the previous paragraph, the Tm and Dy magnetic moment directions used for the theoretical calculations were assigned according to the easy magnetization directions $\langle 110 \rangle$ for $TmAl_2$ and $\langle 001 \rangle$ for $DyAl_2$. Considering much larger value of the Dy-Dy exchange parameter (Table 1) and, consequently, stronger molecular field, the Dy sublattice should dominate the selection of the easy direction in $Tm_xDy_{1-x}Al_2$ compounds studied here (also see below). Hence, to model heat capacity in the 2 T applied field, the magnetic field vector was chosen parallel to the $\langle 001 \rangle$ direction for all values of x. Minor discrepancies between the experimental data and modeling results are both expected and obvious, especially in $\mu_0 H$ = 2 T because the measurements were performed using polycrystalline samples.

Considering that the easy magnetization directions of the parent binary compounds are different, it is important to understand how they compete when Tm and Dy are statistically distributed across the same crystallographic sublattice. Figure 2 shows the temperature dependence of the angle, θ, between the magnetic moments and the crystallographic z axis (the easy direction of $DyAl_2$), in each magnetic sublattice with the 2 T magnetic field applied along the two other main crystallographic cubic directions: $\langle 111 \rangle$ and $\langle 110 \rangle$. The angle θ is calculated from the magnetization components, taken from equation (4), as $\theta(T, \mu_0 H) = \tan^{-1}\left[\sqrt{M_x^2 + M_y^2}/M_z\right]$. We also simulated the temperature dependence of θ with the 2 T magnetic field vector along $\langle 001 \rangle$ direction (data not shown here), and in this case, the magnetic sub-lattices for all three compounds remain fully aligned with the z-axis in the whole temperature range. These results show that $\langle 001 \rangle$ is the easy magnetization direction for all studied pseudobinary compounds.

For x = 0.25 and 0.50, the influence of Dy on the Tm sublattices is dominant, as expected. Even when the magnetic field is applied along $\langle 110 \rangle$, which is the easy magnetization direction of $TmAl_2$, the Tm sublattice is not fully aligned with $\langle 110 \rangle$ at low temperatures, and $\theta \neq 90°$ until the reorientation in the Dy sublattices is complete at $T_R \sim 21$ K and $T_R \sim 12$ K (Fig. 2a and c). In a conventional spin reorientation (SR) process, both sublattices are expected to rotate toward the magnetic field direction when temperature increases until they align along the magnetic field direction at $T = T_R$. However, torque created by the stronger molecular field of Dy makes the SR

process anomalous, where the magnetic moments of Tm initially (between 0 and ~8, and 0 and ~7 K for $x = 0.25$ and $x = 0.5$, respectively) move away from the easy magnetization direction of $TmAl_2$, while approaching the direction of the magnetic moments of Dy. Between 8-21 K and 7-12 K for x = 0.25 and x = 0.50, respectively, the SR process remains anomalous as both magnetic sublattices continue to approach each other, even though they begin to tilt toward the magnetic field direction. In lower, 0.5 and 1 T magnetic fields (supplementary material, Figure S2), the behaviors remain similar to those illustrated in Figs. 2a and 2c. For $x = 0.75$, when the 2 T field is applied along $\langle 110 \rangle$, both sublattices remain fully aligned with the field direction (Fig. 2e). In magnetic fields of 0.5, 1, and 2 T, magnetization along $\langle 001 \rangle$ is the highest when compared to two other examined directions, hence the easy magnetization axis when $x = 0.75$ is also $\langle 001 \rangle$.

When a 2 T magnetic field is applied along the $\langle 111 \rangle$ direction (see Fig. 2b), both magnetic sublattices are nearly aligned along the magnetic field vector at low temperatures when x = 0.25. In a lower magnetic field (0.5 T, supplementary material), a discontinuous SR occurs at T = 21.9 K where the moments in the Dy sublattice become nearly parallel to $\langle 001 \rangle$ with θ_{Tm} closely following behind. For 21.9 K < T < $T_R \cong$ 42 K, both θ_{Dy} (faster) and θ_{Tm} (slower) rotate toward the field direction. This SR process is anomalous since the Tm magnetic moment tilts closer toward that of Dy. With 1 T field parallel to $\langle 111 \rangle$ the behavior (supplementary material) becomes identical to that shown in Fig. 2b. For x = 0.5 and 0.75, in $\mu_0 H = 2\ T$ (Figs. 2d and 2f), on the other hand, the magnetic moments of the Dy sublattices progressively rotate toward the field direction until sharp SR transitions occur at $T_R \cong$ 17.3 K and $T_R \cong$ 6.7 K for $x = 0.5$ and 0.75, respectively. A similar but weaker than for x = 0.25 (Fig. 2a) SR process anomaly is seen for $x = 0.5$ in the inset of Fig. 2d, when θ_{Tm} begins to approach θ_{Dy} starting from ~8.5 K, as marked by the dotted line, continuing until $T_R \sim$ 17.3 K. Hence, with this magnetic field vector orientation, the anomalous SR process (see previous paragraph) is observed for both $x = 0.25$ and $x = 0.5$, but not for $x = 0.75$ compounds (compare insets in Figs. 2d and 2f). Values of T_R for all compounds in magnetic fields of 0.5, 1, and 2 T applied along $\langle 110 \rangle$ and $\langle 111 \rangle$ are listed in the supplementary material, Table S1.

Figures 3 and 4 show the temperature dependencies of the MCE parameters, $-\Delta S_T$ and ΔT_{ad}, respectively, for the magnetic field change from 0 to 2 T calculated with the magnetic field vector along the three main cubic crystallographic directions: $\langle 110 \rangle$ (Fig. 3a and Fig. 4a), $\langle 111 \rangle$ (Fig. 3b and Fig. 4b) and $\langle 001 \rangle$ (Fig. 3c and Fig. 4c), for the $Tm_xDy_{1-x}Al_2$ series with $x = 0.25, 0.50$, and 0.75. The inverse MCEs (related to the rate of change of magnetization with temperature [20,46,47]), observed in Figs. 3a, 3b, 4a, and 4b are associated with the anomalous spin reorientation processes described above. Since $\langle 001 \rangle$ is the easy magnetization direction for three compositions examined in this work, the magnetocaloric effect remains conventional at all temperatures as seen in Figs. 3c and 4c.

The comparison between experimental (symbols) and theoretical (solid lines) isothermal entropy change vs. temperature curves is shown in Figure 5 for the three compounds $Tm_{0.25}Dy_{0.75}Al_2$ (a), $Tm_{0.5}Dy_{0.5}Al_2$ (b), and $Tm_{0.75}Dy_{0.25}Al_2$ (c), upon two different magnetic field changes (0 - 1 T and 0 - 2 T). The theoretical curves were calculated considering the field applied in the easy direction $\langle 001 \rangle$, while the experimental results are obtained using heat capacity (Fig. 1) of the polycrystalline

samples. Theory qualitatively reproduces the shape but the values are higher compared with the experimental data, which at least partially is due to the fact that the model is for single crystals with the magnetic field vector along the easy magnetization axis while experimental data are taken for the polycrystalline samples. Another factor is that experimental data are usually affected by demagnetization, and hence the internal magnetic field is lower than the external applied field [48].

5. Final comments

As a result of this study we were able to model thermomagnetic and magnetocaloric properties of the $Tm_xDy_{1-x}Al_2$ series of compounds with x = 0.25, 0.5, and 0.75 using a Hamiltonian that includes contributions from Zeeman effect, exchange interactions (in the mean field approximation), and crystalline electric field. Other than the observed discrepancies in the ΔS_T values, the general behaviors and the critical temperatures are in good agreement with the experimental values. From temperature dependencies of the orientations of magnetic moments of the lanthanides in the presence of magnetic field it was possible to demonstrate how the spin reorientation occurs for each magnetic sublattice individually, as well as to show how both sublattices are coupled with each other and, consequently, how the coupling influences the magnetocaloric effect. It is worth noting that there is an ongoing work to reproduce theoretically the spin reorientation observed experimentally in the heat capacity of Tm-rich alloys with $x > 0.85$ [32]. Apparently, the magnetic moments of the $TmAl_2$ sublattice are canted in a ferromagnetic phase stable below 3 K as described in references [29, 42].

Acknowledgments

The Ames Laboratory is operated for the U. S. Department of Energy (DOE) by Iowa State University of Science and Technology under contract No. DE-AC02-07CH11358. This work was supported by the Materials Sciences and Engineering Division of the Office of Basic Energy Sciences, Office of Science of the U.S. DOE. This study was also financed in part by the Coordenação de Aperfeiçoamento de Pessoal de Nível Superior – Brasil (CAPES) – Finance Code 001, CNPq – Conselho Nacional de Desenvolvimento Científico e Tecnológico – Brazil and FAPERJ - Fundação de Amparo à Pesquisa do Estado do Rio de Janeiro, which supported POR and BPA stay in Ames. The authors would like to thank Dr. C.M. Bonilla for making the samples used in the heat capacity measurements.

References

[1] K.A. Gschneidner, V.K. Pecharsky, Thirty years of near room temperature magnetic cooling: Where we are today and future prospects, Int. J. Refrig. 31 (2008) 945–961. https://doi.org/10.1016/j.ijrefrig.2008.01.004.

[2] B.G. Shen, J.R. Sun, F.X. Hu, H.W. Zhang, Z.H. Cheng, Recent Progress in Exploring Magnetocaloric Materials, Adv. Mater. 21 (2009) 4545–4564. https://doi.org/10.1002/adma.200901072.

[3] S.P. Alpay, J. Mantese, S. Trolier-McKinstry, Q. Zhang, R.W. Whatmore, Next-generation electrocaloric

and pyroelectric materials for solid-state electrothermal energy interconversion, MRS Bull. 39 (2014) 1099–1111. https://doi.org/10.1557/mrs.2014.256.
[4] X. Moya, E. Defay, V. Heine, N.D. Mathur, Too cool to work, Nat. Phys. 11 (2015) 202–205. https://doi.org/10.1038/nphys3271.
[5] J. Slaughter, A. Czernuszewicz, L. Griffith, V. Pecharsky, Compact and efficient elastocaloric heat pumps—Is there a path forward?, J. Appl. Phys. 127 (2020) 194501. https://doi.org/10.1063/5.0003275.
[6] V. Franco, J.S. Blázquez, J.J. Ipus, J.Y. Law, L.M. Moreno-Ramírez, A. Conde, Magnetocaloric effect: From materials research to refrigeration devices, Prog. Mater. Sci. 93 (2018) 112–232. https://doi.org/10.1016/j.pmatsci.2017.10.005.
[7] E. Brück, Developments in magnetocaloric refrigeration, J. Phys. D. Appl. Phys. 38 (2005) R381–R391. https://doi.org/10.1088/0022-3727/38/23/R01.
[8] O. Gutfleisch, M.A. Willard, E. Brück, C.H. Chen, S.G. Sankar, J.P. Liu, Magnetic Materials and Devices for the 21st Century: Stronger, Lighter, and More Energy Efficient, Adv. Mater. 23 (2011) 821–842. https://doi.org/10.1002/adma.201002180.
[9] G. V. Brown, Magnetic heat pumping near room temperature, J. Appl. Phys. 47 (1976) 3673–3680. https://doi.org/10.1063/1.323176.
[10] V.K. Pecharsky, K.A. Gschneidner Jr, Magnetocaloric effect and magnetic refrigeration, J. Magn. Magn. Mater. 200 (1999) 44–56. https://doi.org/10.1016/S0304-8853(99)00397-2.
[11] A.S. Mischenko, Q. Zhang, J.F. Scott, R.W. Whatmore, N.D. Mathur, Giant electrocaloric effect in thin-film $PbZr_{0.95}Ti_{0.05}O_3$, Science (80-.). 311 (2006) 1270–1271. https://doi.org/10.1126/science.1123811.
[12] T. Strässle, A. Furrer, P. Lacorre, K.A. Müller, A novel principle for cooling by adiabatic pressure application in rare-earth compounds, J. Alloys Compd. 303–304 (2000) 228–231. https://doi.org/10.1016/S0925-8388(00)00662-9.
[13] J. Cui, Y. Wu, J. Muehlbauer, Y. Hwang, R. Radermacher, S. Fackler, M. Wuttig, I. Takeuchi, Demonstration of high efficiency elastocaloric cooling with large ΔT using NiTi wires, Appl. Phys. Lett. 101 (2012) 073904. https://doi.org/10.1063/1.4746257.
[14] P. Weiss, A. Piccard, Le phénomène magnétocalorique, J. Phys. Théorique Appliquée. 7 (1917) 103–109. https://doi.org/10.1051/jphystap:019170070010300.
[15] P. Debye, Einige Bemerkungen zur Magnetisierung bei tiefer Temperatur, Ann. Phys. 386 (1926) 1154–1160. https://doi.org/10.1002/andp.19263862517.
[16] W.F. Giauque, A Thermodynamic treatment of certain magnetic effects. A proposed method of producing temperatures considerably below 1° absolute, J. Am. Chem. Soc. 49 (1927) 1864–1870. https://doi.org/10.1021/ja01407a003.
[17] W.F. Giauque, D.P. MacDougall, Attainment of temperatures below 1°absolute by demagnetization of $Gd_2(SO_4)_3 \cdot 8H_2O$ [12], Phys. Rev. 43 (1933) 768. https://doi.org/10.1103/PhysRev.43.768.
[18] V.K. Pecharsky, K.A. Gschneidner, Giant magnetocaloric effect in $Gd_5(Si_2Ge_2)$, Phys. Rev. Lett. 78 (1997) 4494–4497. https://doi.org/10.1103/PhysRevLett.78.4494.
[19] K.A. Gschneidner, V.K. Pecharsky, Magnetic refrigeration materials (invited), J. Appl. Phys. 85 (1999) 5365–5368. https://doi.org/10.1063/1.369979.
[20] K.A. GschneidnerJr, V.K. Pecharsky, A.O. Tsokol, Recent developments in magnetocaloric materials, Reports Prog. Phys. 68 (2005) 1479–1539. https://doi.org/10.1088/0034-4885/68/6/R04.
[21] X. Moya, S. Kar-Narayan, N.D. Mathur, Caloric materials near ferroic phase transitions, Nat. Mater. 13 (2014) 439–450. https://doi.org/10.1038/nmat3951.
[22] T. Chabri, A. Ghosh, S. Nair, A.M. Awasthi, A. Venimadhav, T.K. Nath, Effects of the thermal and magnetic paths on first order martensite transition of disordered $Ni_{45}Mn_{44}Sn_9In_2$ Heusler alloy exhibiting a giant magnetocaloric effect and magnetoresistance near room temperature, J. Phys. D. Appl. Phys. 51 (2018) 195001. https://doi.org/10.1088/1361-6463/aaba9b.
[23] N.A. Zarkevich, D.D. Johnson, V.K. Pecharsky, High-throughput search for caloric materials: the CaloriCool approach, J. Phys. D. Appl. Phys. 51 (2018) 024002. https://doi.org/10.1088/1361-6463/aa9bd0.
[24] T. Hashimoto, T. Kuzuhara, K. Matsumoto, M. Sahashi, K. Imonata, A. Tomokiyo, H. Yayama, A new method of producing the magnetic refrigerant suitable for the ericsson magnetic refrigeration, IEEE Trans. Magn. 23 (1987) 2847–2849. https://doi.org/10.1109/TMAG.1987.1065717.
[25] F.W. Wang, X.X. Zhang, F.X. Hu, Large magnetic entropy change in $TbAl_2$ and $(Tb_{0.4}Gd_{0.6})Al_2$, Appl. Phys. Lett. 77 (2000) 1360–1362. https://doi.org/10.1063/1.1290389.

[26] P.O. Ribeiro, B.P. Alho, T.S.T. Alvarenga, E.P. Nóbrega, V.S.R. de Sousa, A.M.G. Carvalho, A. Caldas, P.H.O. Lopes, P.J. von Ranke, The influence of crystalline electrical field on magnetic and magnetocaloric properties in $Er_{1-y}Tb_yAl_2$ compounds, J. Magn. Magn. Mater. 442 (2017) 265–269. https://doi.org/10.1016/j.jmmm.2017.06.120.

[27] T. Inoue, S.G. Sankar, R.S. Craig, W.E. Wallace, K.A. Gschneidner, Low temperature heat capacities and thermal properties of $DyAl_2$, $ErAl_2$ and $LuAl_2$, J. Phys. Chem. Solids. 38 (1977) 487–497. https://doi.org/10.1016/0022-3697(77)90182-2.

[28] P. von Ranke, V. Pecharsky, K. Gschneidner, Influence of the crystalline electrical field on the magnetocaloric effect of $DyAl_2$, $ErAl_2$ and $DyNi_2$, Phys. Rev. B - Condens. Matter Mater. Phys. 58 (1998) 12110–12116. https://doi.org/10.1103/PhysRevB.58.12110.

[29] A.F. Deutz, H.B. Brom, W.J. Huiskamp, L.J. de Jongh, K.H.J. Buschow, Low temperature specific heat and a.c. susceptibility of $TmAl_2$, Solid State Commun. 68 (1988) 803–806. https://doi.org/10.1016/0038-1098(88)90068-3.

[30] M. Patra, S. Majumdar, S. Giri, Y. Xiao, T. Chatterji, Magnetocaloric effect in RAl_2 (R=Nd, Sm, and Tm): Promising for cryogenic refrigeration close to liquid helium temperature, J. Alloys Compd. 531 (2012) 55–58. https://doi.org/10.1016/j.jallcom.2012.03.076.

[31] J.C. Patiño, N.A. de Oliveira, P.J. von Ranke, Anisotropic magnetocaloric effect in $TmAl_2$ single crystal, J. Appl. Phys. 116 (2014) 203905. https://doi.org/10.1063/1.4902890.

[32] A.K. Pathak, C.M. Bonilla, D. Paudyal, Y. Mudryk, V.K. Pecharsky, Anomalous specific heat and magnetic properties of $Tm_xDy_{1-x}Al_2$ ($0 \leq x \leq 1$), J. Alloys Compd. 774 (2019) 321–330. https://doi.org/10.1016/j.jallcom.2018.09.365.

[33] V.S.R. de Sousa, E.J.R. Plaza, M.S. Reis, B.P. Alho, A.M.G. Carvalho, S. Gama, N.A. de Oliveira, P.J. von Ranke, Investigation on the magnetocaloric effect in $DyNi_2$, $DyAl_2$ and $Tb_{1-n}Gd_nAl_2$ (n=0, 0.4, 0.6) compounds, J. Magn. Magn. Mater. 321 (2009) 3462–3465. https://doi.org/10.1016/j.jmmm.2009.06.054.

[34] S. Horn, M. Loewenhaupt, H. Scheuer, F. Steglich, Magnetic order and crystal fields in $TmAl_2$ and disordered (Tm, La)Al_2 alloys, J. Magn. Magn. Mater. 14 (1979) 239–240. https://doi.org/10.1016/0304-8853(79)90128-8.

[35] G.X. Tang, W. Nolting, Magnetic properties of disordered Heisenberg binary spin system with long-range exchange, Phys. Rev. B. 73 (2006) 024415. https://doi.org/10.1103/PhysRevB.73.024415.

[36] N.A. de Oliveira, Magnetocaloric effect in rare earth doped compounds, J. Alloys Compd. 455 (2008) 81–86. https://doi.org/10.1016/j.jallcom.2007.01.141.

[37] K.R. Lea, M.J.M. Leask, W.P. Wolf, The raising of angular momentum degeneracy of f-Electron terms by cubic crystal fields, J. Phys. Chem. Solids. 23 (1962) 1381–1405. https://doi.org/10.1016/0022-3697(62)90192-0.

[38] K.W.H. Stevens, Matrix Elements and Operator Equivalents Connected with the Magnetic Properties of Rare Earth Ions, Proc. Phys. Soc. Sect. A. 65 (1952) 209–215. https://doi.org/10.1088/0370-1298/65/3/308.

[39] M.T. Hutchings, Point-Charge Calculations of Energy Levels of Magnetic Ions in Crystalline Electric Fields, in: Solid State Phys. - Adv. Res. Appl., 1964: pp. 227–273. https://doi.org/10.1016/S0081-1947(08)60517-2.

[40] T.W. Hill, W.E. Wallace, R.S. Craig, T. Inoue, Low temperature heat capacities and related thermal properties of $TbAl_2$ and $HoAl_2$, J. Solid State Chem. 8 (1973) 364–367. https://doi.org/10.1016/S0022-4596(73)80036-2.

[41] V.K. Pecharsky, K.A. Gschneidner, Magnetocaloric effect from indirect measurements: Magnetization and heat capacity, J. Appl. Phys. 86 (1999) 565–575. https://doi.org/10.1063/1.370767.

[42] H.G. Purwins, A. Leson, Magnetic properties of (rare earth)Al_2 intermetallic compounds, Adv. Phys. 39 (1990) 309–403. https://doi.org/10.1080/00018739000101511.

[43] D. Kohake, A. Leson, H.G. Purwins, A. Furrer, Magnetization behaviour of $DyAl_2$ single crystals, Solid State Commun. 43 (1982) 965–968. https://doi.org/10.1016/0038-1098(82)90940-1.

[44] W.B. Pearson, The Crystal Chemistry and Physics of Metals and Alloys, New York, 1972.

[45] E.I. Gladyshevsky and O.I. Bodak, Crystal Chemistry of Intermetallic Compounds of Rare Earth Metals (In Russian), Vyshcha Shkola, 1982.

[46] P.J. von Ranke, N.A. de Oliveira, B.P. Alho, E.J.R. Plaza, V.S.R. de Sousa, L. Caron, M.S. Reis, Understanding the inverse magnetocaloric effect in antiferro- and ferrimagnetic arrangements, J. Phys. Condens. Matter. 21 (2009) 056004. https://doi.org/10.1088/0953-8984/21/5/056004.

[47] P.J. von Ranke, B.P. Alho, E.P. Nóbrega, V.S.R. de Sousa, T.S.T. Alvarenga, A.M.G. Carvalho, N.A. de Oliveira, The influence of magnetic and electric coupling properties on the magnetocaloric effect in quantum paraelectric $EuTiO_3$, J. Magn. Magn. Mater. 324 (2012) 1290–1295. https://doi.org/10.1016/j.jmmm.2011.11.037.
[48] C.R.H. Bahl, K.K. Nielsen, The effect of demagnetization on the magnetocaloric properties of gadolinium, J. Appl. Phys. 105 (2009) 013916. https://doi.org/10.1063/1.3056220.

Table 1. Exchange parameters describing the intrasublattice Tm-Tm (λ^{Tm}) and Dy-Dy (λ^{Dy}) interactions, and intersublattice Tm-Dy interactions (λ^{TmDy}).

$\boldsymbol{\lambda^{\mathrm{Tm}}}$ (meV)	$\boldsymbol{\lambda^{\mathrm{Dy}}}$(meV)	$\boldsymbol{\lambda^{\mathrm{TmDy}}}$(meV)
0.036	0.253	0.140

Table 2. Crystalline electric field parameters (from Refs. [31,42]).

Compound	W (meV)	X	$\boldsymbol{F_4}$	$\boldsymbol{F_6}$
$TmAl_2$	0.034	0.48	60	7560
$DyAl_2$	- 0.011	0.30	60	13860

Figure Captions

Figure 1. Heat capacity vs. temperature measured in 0 and 2 T applied magnetic fields for the $Tm_xDy_{1-x}Al_2$ series of compounds with $x = 0.25$ (a), 0.50 (b), 0.75 (c) using polycrystalline samples. The solid and dotted lines are theoretical predictions and the symbols are experimental results obtained with and without magnetic field.

Figure 2. Temperature dependence of the polar angle (θ) of each magnetic sublattice (Tm and Dy) for $Tm_xDy_{1-x}Al_2$ with $x = 0.25$ (a,b), 0.50 (c,d), 0.75 (e,f) for the 2 T magnetic field applied along $\langle 110 \rangle$ and $\langle 111 \rangle$ directions.

Figure 3. Isothermal entropy change *vs.* temperature for the $Tm_xDy_{1-x}Al_2$ series of compounds ($x = 0.25$, 0.50 and 0.75), calculated upon magnetic field variation from 0 to 2 T applied along three different directions: (a) $\langle 110 \rangle$, (b) $\langle 111 \rangle$ and (c) $\langle 001 \rangle$.

Figure 4. Adiabatic temperature change *vs.* temperature for the $Tm_xDy_{1-x}Al_2$ series of compounds ($x = 0.25$, 0.50 and 0.75), calculated upon magnetic field variation from 0 to 2 T applied along three different directions: (a) $\langle 110 \rangle$, (b) $\langle 111 \rangle$ and (c) $\langle 001 \rangle$.

Figure 5. Comparison of the theoretical and experimental temperature dependencies of the isothermal entropy change of $Tm_xDy_{1-x}Al_2$ compounds ($x = 0.25$, 0.50 and 0.75), determined upon two magnetic field variations: $\mu_0 \Delta H$ = 0 to 1 T and 0 to 2 T. The symbols are the experimental data and the solid lines are the theoretical results with the magnetic field applied along $\langle 001 \rangle$ direction.

Figure 1

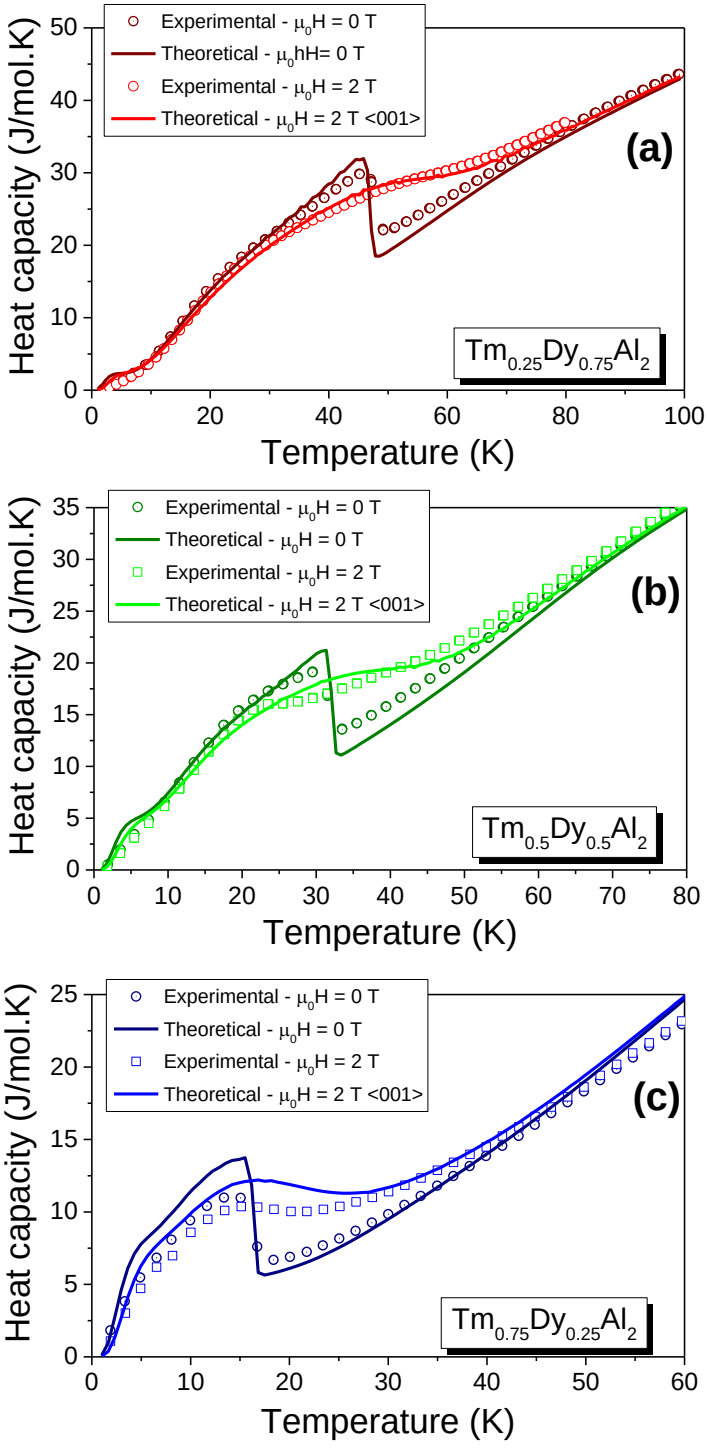
Experimental - μ0H = 0 T
Theoretical - μ0hH= 0 T
Experimental - μ0H = 2 T
Theoretical - μ0H = 2 T <001>
(a)
Tm0.25Dy0.75Al2
Heat capacity (J/mol.K)
Temperature (K)
Experimental - μ0H = 0 T
Theoretical - μ0H = 0 T
Experimental - μ0H = 2 T
Theoretical - μ0H = 2 T <001>
(b)
Tm0.5Dy0.5Al2
Heat capacity (J/mol.K)
Temperature (K)
Experimental - μ0H = 0 T
Theoretical - μ0H = 0 T
Experimental - μ0H = 2 T
Theoretical - μ0H = 2 T <001>
(c)
Tm0.75Dy0.25Al2
Heat capacity (J/mol.K)
Temperature (K)

Figure 2

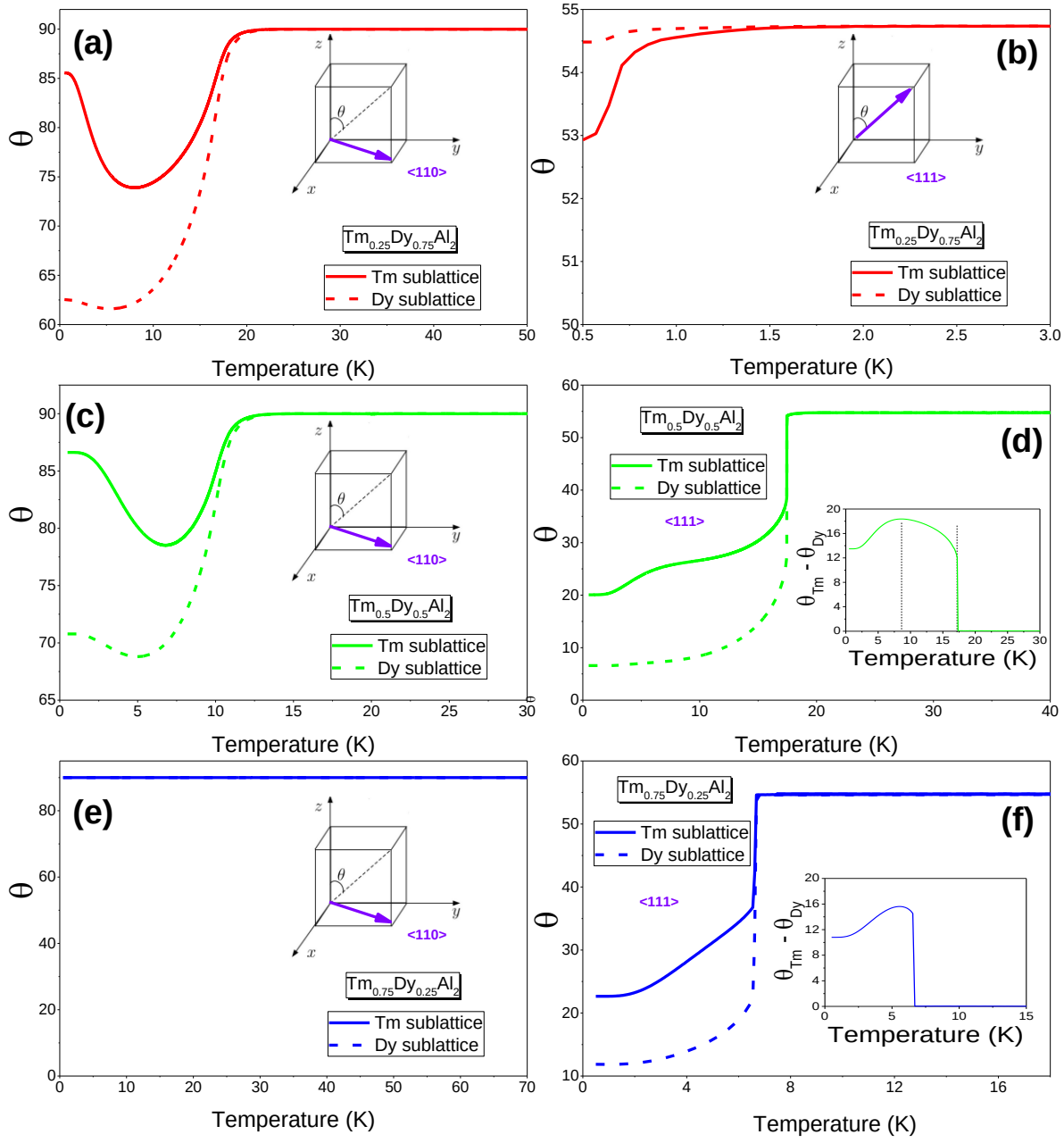
(a)
θ
Temperature (K)
<110>
Tm0.25Dy0.75Al2
Tm sublattice
Dy sublattice
(b)
θ
Temperature (K)
<111>
Tm0.25Dy0.75Al2
Tm sublattice
Dy sublattice
(c)
θ
Temperature (K)
<110>
Tm0.5Dy0.5Al2
Tm sublattice
Dy sublattice
(d)
Tm0.5Dy0.5Al2
Tm sublattice
Dy sublattice
<111>
θTm - θDy
Temperature (K)
θ
Temperature (K)
(e)
θ
Temperature (K)
<110>
Tm0.75Dy0.25Al2
Tm sublattice
Dy sublattice
(f)
Tm0.75Dy0.25Al2
Tm sublattice
Dy sublattice
<111>
θTm - θDy
Temperature (K)
θ
Temperature (K)

Figure 3

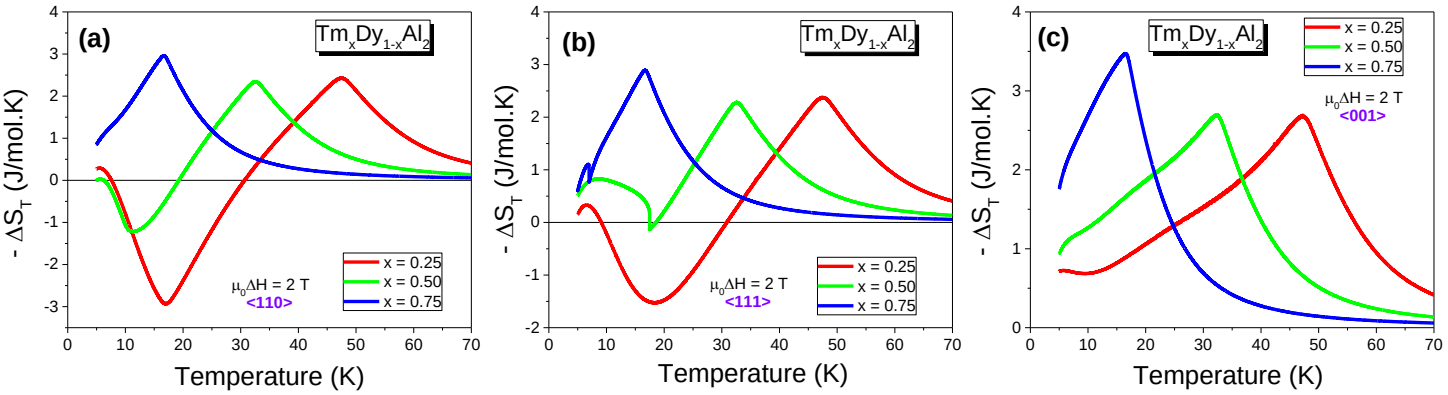

Figure 4

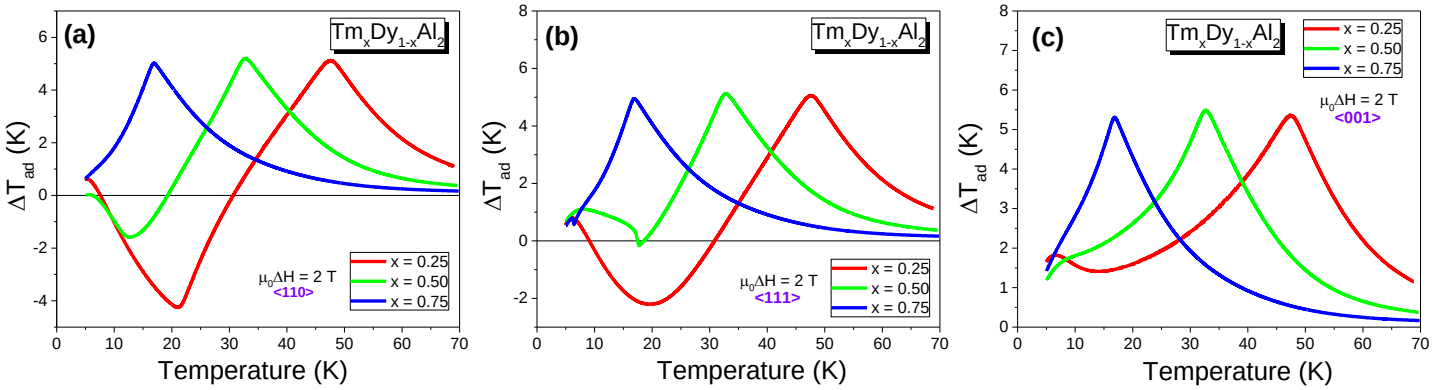

Figure 5